Dalton Transactions

ROYAL SOCIETY OF CHEMISTRY

PAPER

View Article Online
View Journal | View Issue

Cite this: *Dalton Trans.*, 2025, **54**, 14376

Niobium oxyiodide cluster compounds $Li_3Nb_7O_5I_{15}$ and $Nb_8O_5I_{17}(NbI_5)$ with expanding cluster architectures and multicentre Nb–Nb bonding

Jan Beitlberger,[a] Markus Ströbele,[a] Patrick Schmidt,[a] Carl P. Romao[b] and H.-Jürgen Meyer *[a]

Received 30th July 2025,
Accepted 19th August 2025

DOI: 10.1039/d5dt01819f

rsc.li/dalton

A series of niobium oxyiodide compounds has recently been identified using a non-conventional reduction method. The continuation of these studies of heterogeneous solid-state reactions in a closed system has led to the crystallization and structural analysis of two novel compounds $Li_3Nb_7O_5I_{15}$ and $Nb_8O_5I_{17}(NbI_5)$. Both crystal structures are derived from the pentanuclear $[Nb_5O_4]$ cluster core and are expanded through the incorporation of additional niobium atoms, forming new $[Nb_7O_5]$ and $[Nb_8O_5]$ cluster cores. Furthermore, it is shown that oxyiodide clusters containing between four and eight niobium atoms can form from the same mixture of reactants by simply adjusting the composition and temperature. A comprehensive assembly model for these clusters is presented, and electronic structure calculations provide insight into the nature of niobium–niobium bonding within the $[Nb_7O_5]$ core.

Introduction

Metal-rich halide cluster compounds of group 5 and 6 transition metals are well known from the research initiated by the groups of Schäfer, von Schnering and Simon.[1] Preparations of these compounds are typically performed by metallothermic reduction, in which a metal halide (MX_n) is reacted with metal (M), which can be the same metal (M) or an electropositive alkali metal or Al.[2] Attempts to employ non-conventional reduction agents have been demonstrated to provide insights into the reduction pathway (namely through metal intercalation followed by metal halide elimination) by using non-conventional reduction agents, such as Cr, Fe, Co, or Ni, *etc.*, assisted by thermal scanning.[3] Recently, we have successfully employed lithium carbodiimide as a reduction agent, as will be explained subsequently.[4]

The vast majority of transition metal cluster compounds is based on an octahedral cluster core of metal (M) atoms which most commonly appear with $[M_6X_8]$ with eight face-capping X or $[M_6X_{12}]$ with twelve edge-capping X halide (X) environments.[5] In addition, interstitially (Z) stabilized octahedral clusters of the type $[M_6ZX_{12}]$ are reported for *electron-poor* group 4 metals.[6]

More than twenty binary tungsten iodide compounds have been discovered and structurally characterized; most of them are based on the $[M_6X_8]$ type cluster.[7] In contrast, binary niobium iodide compounds involve only Nb_6I_{11}, Nb_3I_8, NbI_3, and NbI_4.[8] An interesting extension of the niobium halide chemistry has been achieved by the employment of an extra non-metal element, leading to heteroanionic cluster compounds, which may provide similar or completely distinct cluster architectures. Thus, heteroanionic clusters can be envisioned to constitute anion replacements in given architectures and to induce a modified structure or connectivity pattern of clusters, as exemplified for Nb_6I_9S (derived from Nb_6I_{11}), Nb_3X_7S (X = Cl, Br, I), and ANb_3Br_7S with A = Rb, Cs (both derived form Nb_3X_8).[9] Different cluster architectures are obtained in compounds with chalcogenides, such as Nb_3TeI_7, $Nb_4Se_4I_4$, $Nb_7S_2I_{19}$, and with pnictide anions in Nb_4PnX_{11} with Pn = N, P, X = Cl, Br, I.[9b,10] Beside the difference in the number of Nb atoms forming the cluster core, the cluster design and connectivity are showing a great variety and so do the properties.

Niobium oxyiodide compounds are reported for $NbOI_3$, NbO_2I, and the metal-rich example $NbOI_2$.[11] Condensed metal–oxide-halides volatilize easily and can be crystallized only within a specific equilibrium window. This observation highlights the sensitivity of these systems to changes in conditions, such as temperature and composition, which can significantly impact the formation of different niobium oxyiodide phases.

The Nb–O–I system was recently a subject of investigations with a focus on metal-rich compounds by employing $Li_2(CN_2)$

[a]*Section for Solid State and Theoretical Inorganic Chemistry, Institute of Inorganic Chemistry, Auf der Morgenstelle 18, 72076 Tübingen, Germany. E-mail: juergen.meyer@uni-tuebingen.de*
[b]*Department of Materials, Faculty of Nuclear Sciences and Physical Engineering, Czech Technical University, Prague, Trojanova 339, 120 00 Nové Město, Czech Republic*

as a reducing agent. The reaction, *i.e.* the reduction, involves the decomposition of the $(NCN)^{2-}$ ion into C_3N_4, as evidenced by IR spectroscopy.[4b] Previous reactions have shown, that the interplay between NbI_4, $Li_2(CN_2)$ and Li_2O can form a heterogeneous system in which local temperatures have an important impact on the phase formation. As a result, we have already reported the compounds Nb_4OI_{12}, Nb_4OI_{11}, and Nb_4OI_{10} with their crystal structures, all based on the rectangular $[Nb_4O]$ core.[4a] With decreasing iodide content, the series of Nb_4OI_{12-x} compounds is showing structures with increasing connectivity between clusters, increasing electrical conductivities, and an increasing number of electrons from six (x = 2) to eight electrons (x = 0) per cluster. Furthermore, we have conducted a detailed analysis of the properties of oxyiodides of the type $M_5O_4I_{11}$, where M = Nb or Ta.[12]

In continuation of this research, we now present two additional niobium oxyiodides, $Li_3Nb_7O_5I_{15}$ and $Nb_8O_5I_{17}(NbI_5)$, featuring $[Nb_7O_5]$ and $[Nb_8O_5]$ cluster cores, each accommodating 13 electrons available for niobium–niobium bonding.

Results and discussion

Synthesis and crystal structure

In our synthesis, NbI_4 was reacted with $Li_2(CN_2)$ and Li_2O. The specific combination of these reactants (see Experimental section) constitutes a heterogeneous reaction system governed by temperature-dependent equilibria, leading to the formation of various solid and gaseous phases. Within this system, $Li_2(CN_2)$ is proposed to function as an unconventional reducing agent for NbI_4, thereby undergoing decomposition of the $(CN_2)^{2-}$ anion to form C_3N_4.

To gain insight into the reaction mechanism, we performed a series of reactions at different temperatures and durations. Heating the mixture to 300 °C yielded an unknown crystalline phase, along with LiI, $NbOI_2$, and an amorphous powder, as determined by powder X-ray diffraction (PXRD) (see Fig. S1, SI). Upon heating at 400 °C for 1 hour, the unidentified phase disappeared, and the compound $Li_3Nb_7O_5I_{15}$ was formed, accompanied by $NbOI_2$ and NbI_5. Prolonged heating at 400 °C for 24 hours resulted in the crystallization of the known $Nb_5O_4I_{11}$, which contains the $[Nb_5O_4]$ cluster core.[12]

Further heating at 500 °C for 1 hour produced crystals characterized as $Nb_8O_5I_{17}(NbI_{5.37})$, which were found on the walls of the ampoule. Extending the heating time at 500 °C to 24 hours led to the formation of Nb_4OI_{10}, a previously reported compound featuring a $[Nb_4O]$ cluster core.[4a]

These results, while focused on solid-state products, do not account for the role of gaseous species that significantly influence the formation pathways of the observed materials. A quenching experiment of the gas phase from 400 °C to room temperature revealed the presence of a black fluid that appeared as small droplets on the ampoule walls (Fig. S2a). After 48 hours at ambient temperature, these droplets transformed into dark red, filamentous crystallites (Fig. S2b), which subsequently decomposed over time (Fig. S2c).

The two new compounds presented in this study, $Li_3Nb_7O_5I_{15}$ and $Nb_8O_5I_{17}(NbI_{5.37})$, were structurally characterized by single-crystal X-ray diffraction (see Table 1). $Li_3Nb_7O_5I_{15}$ crystallizes as rod-like crystals, whereas $Nb_8O_5I_{17}(NbI_{5.37})$ forms plate-like crystals. Several single crystals of the latter were refined, and in each case, the iodide content of the enclosed NbI_5 molecules were found to have slightly more than five iodide atoms, associated with the presence of some polyiodide. For clarity and simplicity, this compound will hereafter be referred to as $Nb_8O_5I_{17}(NbI_5)$.

The crystal structure of $Li_3Nb_7O_5I_{15}$ features an oxygen-stabilized Nb_7 cluster arrangement, in which a central niobium atom (Nb2) is surrounded by six additional niobium atoms (Nb1 and Nb3), forming a trigonal prismatic coordination environment around Nb2 (Fig. 1).

Cluster cores composed of seven metal atoms are relatively rare and often adopt significantly different geometries compared to the $[Nb_7O_5]$ cluster core observed in $Li_3Nb_7O_5I_{15}$. For instance, in $[N(PPh_3)_2][Os_6Au(CO)_{20}H_2]$, the $[Os_6Au]$ cluster is described as two butterfly-shaped units sharing a wing tip.[13] Another example is the asymmetric $[MoFe_6]$ cluster core in

Table 1 Crystallographic and refinement data of $Li_3Nb_7O_5I_{15}$ and $Nb_8O_5I_{17}(NbI_5)$

	$Li_3Nb_7O_5I_{15}$	$Nb_8O_5I_{17}(NbI_{5.37})$
CCDC	2311571	2428720
Space group	*Cmcm*	*Pnma*
Temperature/K	230	200
Unit cell dimensions/Å	a = 14.5783(3)	a = 11.4282(4)
	b = 17.6445(3)	b = 13.4336(6)
	c = 13.5823(2)	c = 31.479(1)
Volume/Å^3	3493.7(1)	4848.1(3)
Z	4	4
Wavelength/Å	1.54184	1.54184
μ/mm^{-1}	122.292	128.729
2θ range for data collection	7.866 to 136.454	5.598 to 133.306
Total number of reflections	17 730	47 074
Independent reflections	1742	4437
Refined parameters	85	240
R_{int}	0.0316	0.0589
R_1	0.0197	0.0274
wR_2	0.0534	0.0516
Goodness-of-fit on F^2	1.060	1.036

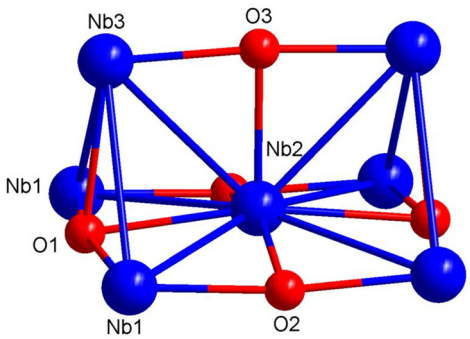

Fig. 1 Structure of the $[Nb_7O_5]$ cluster core inside $Li_3Nb_7O_5I_{15}$.

$[Ph_4As]_2[MoFe_6S_6(CO)_{16}]$.[14] Octahedral M_6 clusters containing a central transition-metal atom are also known, particularly among rare-earth and zirconium-based compounds.[15]

In contrast, the $[Nb_7O_5]$ cluster core can be regarded as an extension to the $[M_5O_4]$ cluster core found in the $M_5O_4I_{11}$ compounds (M = Nb, Ta) through addition of three more atoms, namely two Nb3 atoms and the O3 ion depicted in Fig. 1. The $[Nb_7O_5]$ cluster core represents six short Nb–Nb distances between the central Nb2 with the surrounding six niobium atoms measuring 2.7883(7) Å (Nb2–Nb3) and 2.8050(4) Å (Nb1–Nb2). These distances are significantly shorter than the Nb1 and Nb3 separation, which measure 3.0667(6) Å. The cluster is surrounded by iodide ligands, including four edge-capping ligands, four terminal ligands, and twelve iodide ligands that bridge between adjacent cluster cores in a 12/2 fashion, as illustrated in Fig. 2. Using the notation originally developed for octahedral cluster compounds, distinguishing between inner (i), outer (a), and outer-bridging (a–a) ligand functionalities, the connectivity pattern of the cluster can be described as $(Nb_7O_5I_4^{i})I_4^{a}I_{12/2}^{a-a}$.

This cluster fragment is further stabilized by three lithium ions and one additional iodide ion, completing the overall formula $Li_3Nb_7O_5I_{15}$. Four outer iodide ligands from the cluster, along with the additional iodide ion (I5), surround each lithium ion (Li1 and Li2) in a square-pyramidal fashion (see Fig. 3). The less flexible cluster-bound iodide ligands (I2 and I3) form the base of the square pyramid, with Li–I distances ranging from 2.904(6) to 3.17(1) Å, while the more flexible additional iodide ion (I5) occupies the apical position, showing Li–I distances of 2.64(2) Å and 2.76(1) Å.

The complete structure of $Li_3Nb_7O_5I_{15}$ is constructed by linking each $[Nb_7O_5]$ cluster to six neighbouring clusters, forming a three-dimensional framework. As illustrated in Fig. 4, a view along the *c*-axis of the structure reveals an alternating orientation of the adjacent clusters, highlighting the spatial arrangement and connectivity within the extended structure.

The second cluster compound obtained from the same basic reaction is $Nb_8O_5I_{17}(NbI_5)$. The $[Nb_8O_5]$ cluster core contained within this compound can be viewed as an extension of the $[Nb_7O_5]$ core found in $Li_3Nb_7O_5I_{15}$, incorporating just one additional niobium atom. As shown in Fig. 5, this extension occurs through the addition of a niobium atom (Nb5) positioned at one edge of the $[M_5O_4]$ base, effectively expanding the cluster architecture.

As observed for the previously discussed $[Nb_7O_5]$ cluster core, the Nb–Nb distances between the central Nb2 atom and the six surrounding niobium atoms (Nb1, Nb3, Nb4) in $Nb_8O_5I_{17}(NbI_5)$ are relatively short, ranging from 2.7911(3) to 2.8600(7) Å. In contrast, the Nb–Nb distances between Nb3–Nb1 and Nb3–Nb4 are notably longer, falling in the range of 2.9981(6) to 3.1812(7) Å. The Nb–Nb distance involving the additional Nb5 atom is with 3.1418(7) Å in the same range. A comprehensive comparison of Nb–O bond lengths for both compounds is provided in Table 2. This comparison shows a good overall agreement between the structural metrics observed in the two cluster compounds.

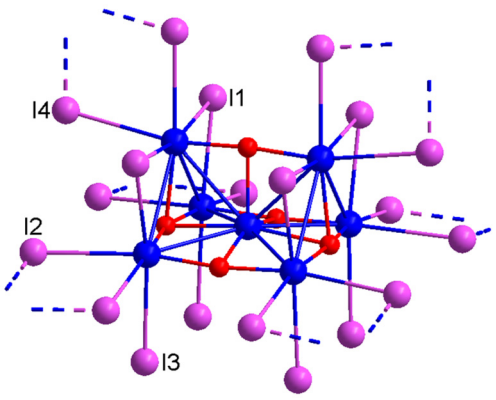

Fig. 2 Iodide coordination of the $[Nb_7O_5]$ cluster core, with twelve iodide atoms having bridging functionality (indicated by dashed lines). Niobium atoms are coloured in blue, oxygen in red and iodine in pink.

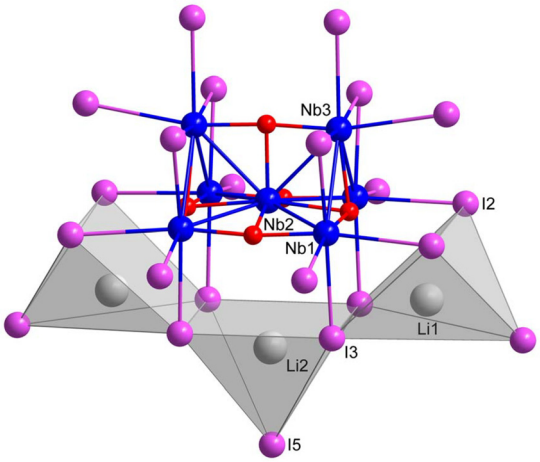

Fig. 3 Square-pyramidal lithium (grey) coordination in the structure with the additional iodide atom (I5).

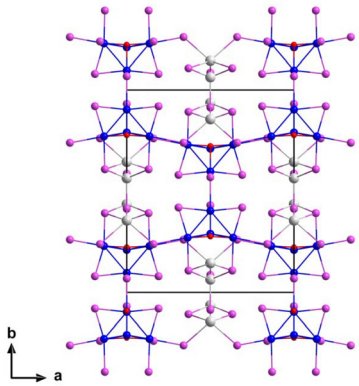

Fig. 4 Projection of the crystal structure of $Li_3Nb_7O_5I_{15}$, looking along the *c*-axis. Niobium atoms are shown in blue, oxygen in red, iodine in pink and lithium in grey.

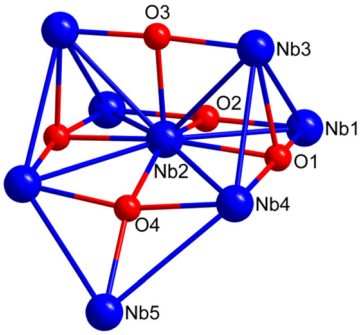

Fig. 5 The $[Nb_8O_5]$ cluster core of $Nb_8O_5I_{17}(NbI_5)$.

Table 2 Nb–O distances in the cluster cores of the two compounds and the average Nb–O distances with the corresponding coordination number (CN) of the oxygen

Compound distance/Å	$Li_3Nb_7O_5I_{15}$	$Nb_8O_5I_{17}(NbI_5)$
Nb1–O1	2.0005(9)	1.958(5)
Nb1–O2	1.9568(5)	1.9564(6)
Nb2–O1	2.197(6)	2.205(6)
Nb2–O2	2.097(6)	2.093(8)
Nb2–O3	2.080(8)	2.079(7)
Nb2–O4		2.084(7)
Nb3–O1	2.247(6)	2.233(5)
Nb3–O3	1.9464(6)	1.9415(7)
Nb4–O1		2.010(5)
Nb4–O4		2.122(1)
Nb5–O4		2.073(7)
∅ Nb–O1 (CN = 4)	2.11(1)	2.10(1)
∅ Nb–O2 (CN = 3)	2.00(1)	2.00(1)
∅ Nb–O3 (CN = 3)	1.99(1)	1.99(1)
∅ Nb–O4 (CN = 4)		2.10(1)

The presence of the additional niobium atom in the structure $Nb_8O_5I_{17}(NbI_5)$ alters, both the local environment and the connectivity pattern of the cluster. The connectivity changes from $(Nb_7O_5I_4^{i})I_4^{a}I_{12/2}^{a-a}$ in $Li_3Nb_7O_5I_{15}$ to $(Nb_8O_5I_8^{i})I_5^{a}I_{8/2}^{a-a})$ in $Nb_8O_5I_{17}(NbI_5)$ (Fig. 6). As a result, the number of connections to neighboring clusters is reduced to just four, leading to a dimensional reduction in the overall connectivity, from a three-dimensional framework in $Li_3Nb_7O_5I_{15}$ to a layered arrangement in $Nb_8O_5I_{17}(NbI_5)$ with zig-zag layers extending along the *ab*-plane (Fig. 7).

Between the layers of the $Nb_8O_5I_{17}(NbI_5)$ structure, channels are formed that accommodate NbI_5 units (Fig. S3). The observed disorder in these regions arises from the partial incorporation of excess iodine, likely in the form of coordinated polyiodide species such as I_2^- or I_3^-. These species preferentially align along the crystallographic *a*-axis, contributing to the structural complexity and variability of the interlayer region.

The intercalation of molecular species within a solid-state framework is relatively uncommon but well-documented in the literature. Such molecules can reside in interlayer spaces or structural channels when the host framework provides cavities large enough to accommodate them. A notable example is the crystal structure of $Nb_7S_2I_{19}$, which can be described as $(Nb_3SI_7)_2(NbI_5)$.[10d] In this compound, six $[Nb_3S]$ units form iodide-bridged ring arrangements that create central channels occupied by NbI_5 molecules. Another example is $Ta_5O_4I_{11}(TaI_5)$, where TaI_5 molecules are intercalated between corrugated layers.[12] In this case, TaI_5 acts as a structural template for layer formation, as a similar cluster connectivity is observed in m-$Ta_5O_4I_{11}$. A comparable template effect is reported in $[K_5(Ti_2Cl_9)][(Nb_6Cl_{12}O_4)_3(Ti_3Cl_4)_2]$,[16] where the complex anion $[(Nb_6Cl_{12}O_4)_3(Ti_3Cl_4)_2]^{2-}$ forms a layered framework with large channels, which are filled by $[K_5(Ti_2Cl_9)]^{2+}$ units. A related scenario is found in $Cs_3(ZrCl_5)Zr_6Cl_{15}Mn$,

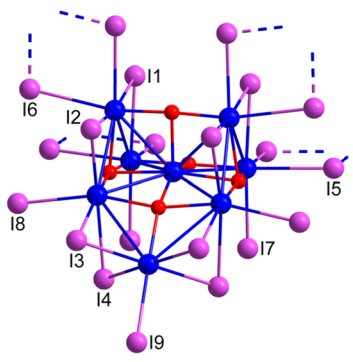

Fig. 6 Iodide coordination of the $[Nb_8O_5]$ cluster core with eight iodide atoms with bridging functionality (indicated by dashed lines) connecting to four adjacent clusters. Niobium atoms are coloured in blue, oxygen in red and iodine in pink.

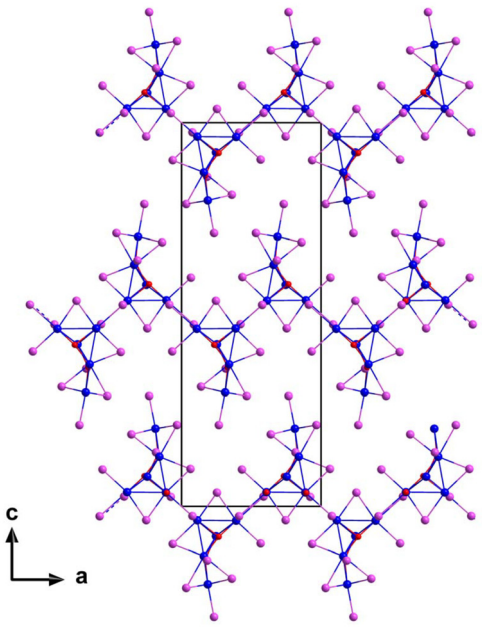

Fig. 7 Projected structure with the $Nb_8O_5I_{17}$ section of $Nb_8O_5I_{17}(NbI_5)$. The NbI_5 molecules between the layers are omitted for clarity. Niobium atoms are shown in blue, oxygen in red and iodine in pink.

where $ZrCl_5^-$ units are incorporated into a three-dimensional framework constructed from $[Zr_6(Mn)Cl_{12}{}^{i}]Cl_{6/2}{}^{a-a}$.[15a] Such a monoanionic molecule can also be intercalated into a simple metal halide, as demonstrated by the compound $(Ta_6Br_{15})(TaBr_6)_{0.86}$.[17] These examples show how molecular species can be stabilized within solid-state matrices by occupying voids or acting as templates that influence framework formation.

Scanning electron microscopy (SEM) and energy dispersive X-ray spectroscopy (EDX)

Scanning electron microscopy was performed with the aid of a custom-designed vacuum transfer device to transfer the samples under inert conditions. Fig. 8 shows some crystals of $Li_3Nb_7O_5I_{15}$, having a rod-like morphology with right-angled edges and a rough surface.

To confirm the composition determined by X-ray diffraction of $Li_3Nb_7O_5I_{15}$, EDX measurements on multiple crystals were performed. These measurements result in an average Nb : I ratio of 7 : 15.2(6).

Electronic band structure and ELF calculations

The electronic structure of $Li_3Nb_7O_5I_{15}$ was investigated using density functional theory (DFT). The calculated band structure, shown in Fig. 9, reveals seven metal-centred energy bands located below the Fermi level. Among these, the highest-energy band intersects the Fermi level at multiple points in the Brillouin zone. These seven bands correspond to one formula unit of $Li_3Nb_7O_5I_{15}$ and primarily arise from niobium–niobium bonding interactions within the $[Nb_7O_5]$ cluster, rather than in between clusters. In total, they accommodate 13 electrons per cluster. However, this number of electrons cannot be straightforwardly assigned to specific niobium–niobium contacts within the cluster core, especially when considering a notably large number of relatively short Nb–Nb distances within the cluster, discussed previously. The presence of a high density of bands at and above the Fermi level indicates delocalization of electrons across these bands. This suggests a more delocalized distribution of bonding interactions across the cluster core.

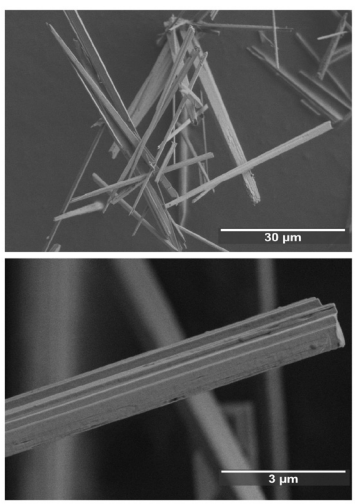

Fig. 8 Scanning electron micrographs of $Li_3Nb_7O_5I_{15}$.

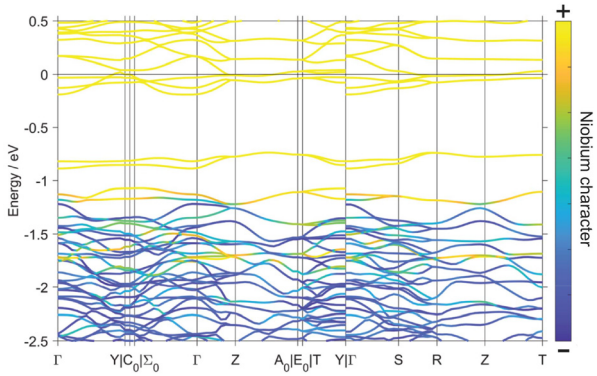

Fig. 9 DFT-calculated electronic band structure of $Li_3Nb_7O_5I_{15}$ with bands coloured by their niobium character. Special points in and paths through the Brillouin zone were chosen following the literature.[18]

Beside the reasonably high niobium content of the bands, there is also some content arising from oxygen orbitals in bands below the Fermi energy (Fig. S4). Hence, there seems to be oxygen states hybridizing with niobium states which leads to some covalent character of some Nb–O bonds. Electron localization function (ELF) calculations of the cluster core support this interpretation. As shown in (Fig. 10, left), there is notable electron density extending from the O1 atom into the Nb1–Nb3 bonding region, indicating participation of oxygen in metal–metal bonding. Furthermore, a pronounced region of electron density is observed between Nb1, Nb2, and Nb3 (Fig. 10, right), consistent with the presence of a three-centred

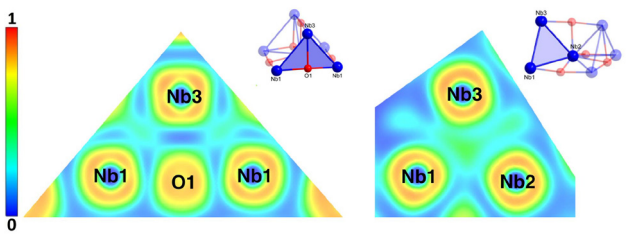

Fig. 10 Electron localisation functions of the $[Nb_7O_5]$ cluster core in $Li_3Nb_7O_5I_{15}$.

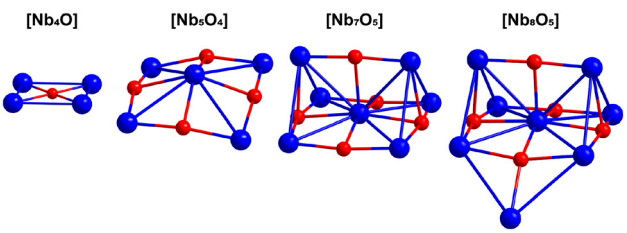

Fig. 11 The expansion of cluster architectures of niobium oxide cluster cores in various niobium oxyiodides.

bond. The ELF analysis suggests the presence of four such three-centred bonds, in addition to four Nb–Nb bonds with an admixture of electron density coming from oxygen within the cluster. These bonding interactions highlight the significant role of orbital mixing between niobium d-orbitals and oxygen p-orbitals in stabilizing the cluster core and the cluster framework.

Conclusion

With the discovery of the niobium oxyiodide cluster compounds $Li_3Nb_7O_5I_{15}$ and $Nb_8O_5I_{17}(NbI_5)$, the family of cluster architectures featuring $[Nb_xO_y]$ cores is expanded by two new members. The smallest cluster in this series is the $[Nb_4O]$ core in Nb_4OI_{12-x}, followed by the $[Nb_5O_4]$ core in $Nb_5O_4I_{11}$, and now the $[Nb_7O_5]$ and $[Nb_8O_5]$ cores reported in the present work. These clusters are illustrated in Fig. 11.

All compounds were synthesized *via* heterogeneous solid-state reactions between NbI_4 and $Li_2(CN_2)$, which served as an unconventional reducing agent, in the presence of an oxide. The formation of the reported compounds occurs *via* temperature-dependent equilibria, influenced by slight variations in composition and the generation of various solid and gaseous phases (Fig. S5). Importantly, the gas phase and the specific gaseous species involved is thought to play a key role in guiding the formation pathways of the resulting cluster compounds.

Experimental section

Materials and methods

All manipulations of starting materials and products were performed in a glovebox under dry argon with moisture and oxygen levels below 1 ppm. Li_2O (ABCR, 95%) was used as purchased. NbI_4 and $Li_2(CN_2)$ were synthesized as described in the literature.[19]

Synthesis

$Li_3Nb_7O_5I_{15}$ was synthesized from NbI_4, Li_2O and $Li_2(CN_2)$. For this purpose, NbI_4 (160.8 mg, 0.268 mmol), Li_2O (2 mg, 0.067 mmol), and $Li_2(CN_2)$ (7.2 mg, 0.135 mmol) were encapsulated into a fused silica ampoule with 3 cm length and a volume of about 1.5 cm^3. The ampoule was heated in a box furnace from room temperature to 500 °C with a rate of 0.1 °C min^{-1}. The holding time was 24 h before the reaction was cooled down to room temperature with a rate of 2 °C min^{-1}. Rod-like crystals of $Li_3Nb_7O_5I_{15}$ were found at the bottom of the ampoule in the powder, beside LiI and an amorphous phase, produced by the decomposition of $Li_2(CN_2)$. The product was washed with dried ethanol to get rid of the LiI. A powder pattern of pure product war recorded (Fig. S6). The estimated yield of $Li_3Nb_7O_5I_{15}$ was about 80%; crystals appear black and decompose in air due to moisture after some time.

$Nb_8O_5I_{17}(NbI_5)$ was synthesized from NbI_4, Li_2O and $Li_2(CN_2)$. For this purpose, NbI_4 (160.8 mg, 0.268 mmol), Li_2O (2 mg, 0.067 mmol) and $Li_2(CN_2)$ (7.2 mg, 0.135 mmol) were encapsulated into a fused silica ampoule with 3 cm length and a volume of about 1.5 cm^3. The ampoule was heated in a Simon-Müller furnace from room temperature to 500 °C with a rate of 0.1 °C. The holding time was 1 h before the reaction was cooled down to room temperature with a rate of 2 °C min^{-1}. Plate-like crystals of $Nb_8O_5I_{17}(NbI_5)$ were found at the wall in the middle of the ampoule with $NbOI_2$ and NbI_5 at the top of the ampoule and LiI, $Li_3Nb_7O_5I_{15}$ and amorphous C_3N_4 in the powder. An X-ray powder pattern of pure product was recorded (Fig. S7). Crystals appear black and decompose in air due to moisture quite fast.

Crystallography

A rod-like $Li_3Nb_7O_5I_{15}$ and a plate-like $Nb_8O_5I_{17}(NbI_5)$ single-crystal were mounted on a Rigaku XtaLab Synergy-S X-ray diffractometer using Cu-K_α (λ = 1.54184 Å) radiation. The single crystal was kept under N_2 cooling at 230 K during the data collection. Corrections for absorption effects were applied with CrysAlisPro 1.171.42.70a (Rigaku Oxford Diffraction, 2022). The crystal structure was solved by the integrated space group and crystal-structure determination routine of SHELXT[20] and full-matrix least-squares refinement with SHELXL-2018/3[20] implemented in Olex2 1.5.[21]

Reaction products were investigated by powder X-ray diffraction (PXRD) using a StadiP diffractometer (Stoe, Darmstadt) with Ge[111]-monochromated Cu-$K_{\alpha1}$ radiation and a Mythen1 detector.

Density functional theory

Density functional theory (DFT) calculations were performed using the Abinit software package (v. 9).[22] The Perdew–Burke–Ernzerhof exchange–correlation functional[23] was used with the vdw-DFT–D3(BJ) dispersion correction of Grimme.[24] A Monkhorst–Pack grid of *k*-points with real-space basis vectors (3 3 0) (−2 2 0) and (0 0 3) was used to construct the electronic structure of crystalline $Li_3Nb_7O_5I_{15}$.[25] Plane-wave calculations were performed using an energy cutoff of 40 Ha outside of the PAW spheres and a 120 Ha cutoff inside them. Pseudopotentials sets were used as received from the Abinit library.[22] These computational parameters were chosen following convergence studies.

Conflicts of interest

The authors declare no conflict of interest.

Data availability

The data that support the findings of this study are available on request from the corresponding author, H.-J. Meyer. Computational data are avaliable at **https://doi.org/10.5281/zenodo.15366543**.

Supplementary information is available. See DOI: https://doi.org/10.1039/d5dt01819f.

CCDC 2311571 ($Li_3Nb_7O_5I_{15}$) and 2428720 ($Nb_8O_5I_{17}(NbI_{5.37})$) contains the supplementary crystallographic data for this paper.[26a,b]

Acknowledgements

This research was supported by the Deutsche Forschungsgemeinschaft (ME 914-32/1) and the state of Baden-Württemberg through bwHPC and the German Research Foundation (DFG) through grant no INST 40/467-1 FUGG (JUSTUS cluster). C. P. R. acknowledges support from the project FerrMion of the Ministry of Education, Youth and Sports, Czech Republic, co-funded by the European Union (CZ.02.01.01/00/22_008/0004591), the European Union and Horizon 2020 through grant no. 810451.

References

1 (*a*) H. Schäfer and H.-G. von Schnering, *Angew. Chem.*, 1964, **76**, 833–849; (*b*) A. Broll, A. Simon, H.-G. von Schnering and H. Schäfer, *Z. Anorg. Allg. Chem.*, 1969, **367**, 1–18.

2 G. Brauer, *Handbuch der Präparativen Anorganischen Chemie*, Ferdinand Enke Verlag, Stuttgart, 1981, vol. 3.

3 (*a*) A. Mos, C. Castro, S. Indris, M. Ströbele, R. F. Fink and H.-J. Meyer, *Inorg. Chem.*, 2015, **54**, 9826–9832; (*b*) A. Mos, M. Ströbele and H.-J. Meyer, *Z. Anorg. Allg. Chem.*, 2015, **641**, 1722–1727; (*c*) A. Mos, M. Ströbele and H.-J. Meyer, *J. Cluster Sci.*, 2015, **26**, 187–198; (*d*) A. Mos-Hummel, M. Ströbele and H.-J. Meyer, *Eur. J. Inorg. Chem.*, 2016, **2016**, 4234–4240.

4 (*a*) J. Beitlberger, M. Ströbele, F. Strauss, M. Scheele, C. P. Romao and H.-J. Meyer, *Eur. J. Inorg. Chem.*, 2024, **27**, e202400329; (*b*) J. Beitlberger, M. Martin, M. Scheele, P. Schmidt, M. Ströbele and H.-J. Meyer, *Dalton Trans.*, 2025, **54**, 5486–5493.

5 L. Pauling, *The Nature of the Chemical Bond and the Structure of Molecules and Crystals: An Introduction to Modern Structural Chemistry*, Cornell University Press, 1960.

6 R. P. Ziebarth and J. D. Corbett, *J. Solid State Chem.*, 1989, **80**, 56–67.

7 M. Ströbele and H.-J. Meyer, *Dalton Trans.*, 2019, **48**, 1547–1561.

8 (*a*) A. Simon and H.-G. von Schnering, *J. Less-Common Met.*, 1966, **11**, 31–46; (*b*) A. Simon, H.-G. von Schnering and H. Schäfer, *Z. Anorg. Allg. Chem.*, 1967, **355**, 295–310; (*c*) P. W. Seabaugh and J. D. Corbett, *Inorg. Chem.*, 1965, **4**, 176–181; (*d*) L. F. Dahl and D. L. Wampler, *Acta Crystallogr.*, 1962, **15**, 903–911.

9 (*a*) H.-J. Meyer and J. D. Corbett, *Inorg. Chem.*, 1991, **30**, 963–967; (*b*) P. J. Schmidt and G. Thiele, *Acta Crystallogr., Sect. C: Cryst. Struct. Commun.*, 1997, **53**, 1743–1745; (*c*) G. V. Khvorykh, A. V. Shevelkov, V. A. Dolgikh and B. A. Popovkin, *J. Solid State Chem.*, 1995, **120**, 311–315; (*d*) C. M. Pasco, Dissertation, Johns Hopkins University, 2021; (*e*) F. Grahlow, F. Strauß, M. Scheele, M. Ströbele, A. Carta, S. F. Weber, S. Kroeker, C. P. Romao and H.-J. Meyer, *Phys. Chem. Chem. Phys.*, 2024, **26**, 11789–11797; (*f*) H.-J. Meyer, *Z. Anorg. Allg. Chem.*, 1994, **620**, 863–866.

10 (*a*) M. Ströbele, O. Oeckler, M. Thelen, R. F. Fink, A. Krishnamurthy, S. Kroeker and H.-J. Meyer, *Inorg. Chem.*, 2022, **61**, 17599–17608; (*b*) M. D. Smith and G. J. Miller, *J. Alloys Compd.*, 1998, **281**, 202–205; (*c*) H. B. Yaich, J. C. Jegaden, M. Potel, M. Sergent, A. K. Rastogi and R. Tournier, *J. Less-Common Met.*, 1984, **102**, 9–22; (*d*) G. J. Miller and J. Lin, *Angew. Chem., Int. Ed. Engl.*, 1994, **33**, 334–336.

11 (*a*) J. Rijnsdorp and F. Jellinek, *J. Less-Common Met.*, 1978, **61**, 79–82; (*b*) S. Hartwig, Dissertation, University of Bayreuth, 2003.

12 F. Grahlow, J. Beitlberger, M. Martin, E. Juriatti, H. Peisert, M. Scheele, M. Ströbele, C. P. Romao and H.-J. Meyer, unpublished work.

13 B. F. G. Johnson, D. A. Kaner, J. Lewis and P. R. Raithby, *J. Chem. Soc., Chem. Commun.*, 1981, 753–755.

14 P. A. Eldredge, K. S. Bose, D. E. Barber, R. F. Bryan, E. Sinn, A. Rheingold and B. A. Averill, *Inorg. Chem.*, 1991, **30**, 2365–2375.

15 (*a*) J. Zhang and J. D. Corbett, *Inorg. Chem.*, 1995, **34**, 1652–1656; (*b*) T. Hughbanks and J. D. Corbett, *Inorg. Chem.*, 1988, **27**, 2022–2026; (*c*) J. Zhang and J. D. Corbett, *Inorg. Chem.*, 1993, **32**, 1566–1572.

16 T. Duraisamy, Y. Zhihua, E. V. Anokhina, C. S. Choi, C. S. Day and A. Lachgar, *J. Solid State Chem.*, 2003, **175**, 46–51.

17 K. Habermehl, A.-V. Mudring and G. Meyer, *Eur. J. Inorg. Chem.*, 2010, **2010**, 4075–4078.

18 Y. Hinuma, G. Pizzi, Y. Kumagai, F. Oba and I. Tanaka, *Comput. Mater. Sci.*, 2017, **128**, 140–184.

19 (*a*) G. Brauer, *Handbuch der präparativen anorganischen Chemie*, Enke, 1975; (*b*) R. Srinivasan, M. Ströbele and H.-J. Meyer, *Inorg. Chem.*, 2003, **42**, 3406–3411.

20 G. M. Sheldrick, *Acta Crystallogr., Sect. C: Struct. Chem.*, 2015, **71**, 3–8.

21 O. V. Dolomanov, L. J. Bourhis, R. J. Gildea, J. A. K. Howard and H. Puschmann, *J. Appl. Crystallogr.*, 2009, **42**, 339–341.

22 X. Gonze, B. Amadon, G. Antonius, F. Arnardi, L. Baguet, J.-M. Beuken, J. Bieder, F. Bottin, J. Bouchet, E. Bousquet, N. Brouwer, F. Bruneval, G. Brunin, T. Cavignac, J.-B. Charraud, W. Chen, M. Côté, S. Cottenier, J. Denier, G. Geneste, P. Ghosez, M. Giantomassi, Y. Gillet, O. Gingras, D. R. Hamann, G. Hautier, X. He, N. Helbig, N. Holzwarth, Y. Jia, F. Jollet, W. Lafargue-Dit-Hauret, K. Lejaeghere, M. A. L. Marques, A. Martin, C. Martins, H. P. C. Miranda, F. Naccarato, K. Persson, G. Petretto, V. Planes, Y. Pouillon, S. Prokhorenko, F. Ricci,

G.-M. Rignanese, A. H. Romero, M. M. Schmitt, M. Torrent, M. J. van Setten, B. Van Troeye, M. J. Verstraete, G. Zérah and J. W. Zwanziger, *Comput. Phys. Commun.*, 2020, **248**, 107042.

23 J. P. Perdew, K. Burke and M. Ernzerhof, *Phys. Rev. Lett.*, 1996, **77**, 3865–3868.

24 S. Grimme, J. Antony, S. Ehrlich and H. Krieg, *J. Chem. Phys.*, 2010, **132**, 154104.

25 H. J. Monkhorst and J. D. Pack, *Phys. Rev. B: Condens. Matter Mater. Phys.*, 1976, **13**, 5188–5192.

26 (*a*) J. Beitlberger, M. Ströbele, P. Schmidt, C. P. Romao and H.-J. Meyer, CCDC 2311571: Experimental Crystal Structure Determination, 2025, DOI: **10.5517/ccdc.csd.cc2hlct9**; (*b*) J. Beitlberger, M. Ströbele, P. Schmidt, C. P. Romao and H.-J. Meyer, CCDC 2428720: Experimental Crystal Structure Determination, 2025, DOI: **10.5517/ccdc.csd.cc2mj8t8**.